On the swimming of a flexible body in a vortex street

S I L A S   A L B E N†

School of Mathematics, Georgia Institute of Technology, Atlanta, GA 30332-0160, USA

We formulate a new theoretical model for the swimming of a flexible body in a vortex street. We consider the class of periodic travelling-wave body motions, in the limit of small amplitude. We calculate the output power provided to the body by thrust forces, and the input power done against pressure forces, as functions of the aspect ratio and strength of the vortex street. We then formulate two optimization problems. In the first, we determine the body wave which provides maximum output power for fixed amplitude. We find a closed-form solution with a transition from power law to exponential decay of output power as the vortex street widens. In the second problem, we incorporate internal viscoelasticity to the swimming body and compute its contribution to the input power. We find the body wave which maximizes efficiency for a given output power. The body shape and resulting efficiency are found in closed form and simple approximate formulas are given. We find that efficiency scales as the inverse of the damping parameter. Finally, we compare our results with previous experiments and simulations. We find agreement in some aspects and disagreement in others. We give physical interpretations for agreements and disagreements in terms of the phase between the body wave and vortex street.

1. Introduction

The interaction between solid bodies and vortices is a central component of many instances of locomotion in fluids. In schools of fish (Weihs 1973; Abrahams & Colgan 1987) and flocks of birds (Lissaman & Shollenberger 1970; Weimerskirch *et al.* 2001) individuals encounter vortical structures created by other individuals, leading to significant changes in the fluid forces they experience. The same phenomenon occurs among the multiple fins of a single swimming fish (Videler 1993; Drucker & Lauder 2001). Tuning the motion of the body in response to oncoming vorticity can lead to significant savings in the energy needed for locomotion.

An inviscid model of an important two-dimensional problem was put forwards by Streitlien, Triantafyllou & Triantafyllou (1996). They considered a Joukowski airfoil heaving and pitching in the flow of an alternating (von Kármán) vortex street, which is a classical model for the wake of a body at Reynolds numbers of $O(10^2 - 10^5)$. They formulated a full numerical model, and a simpler linearized model for the limit of small airfoil motions. The numerical model represents each vortex in the street as a cluster of point vortices spread over a small area. At discrete time steps, new point vortices are released near the trailing edge of the airfoil. The strength of these vortices is set to make the flow velocity finite at the trailing edge (a version of the

† Email address for correspondence: alben@math.gatech.edu

Kutta condition Batchelor 1967). Then they varied heaving and pitching amplitude, frequency and phase parameters, and computed the forces on the airfoil. The analytical model began by computing the instantaneous far-field flow encountered by the airfoil. This flow is the potential flow due to the vortex street at the position of the airfoil, projected onto the centreline between the alternating rows of vortices. This model, related to a model of Wu & Chwang (1975), considers the limit in which the heaving amplitude of the body is small relative to the size and to the vertical and horizontal spacing of the vortices.

Their simulations found that Froude efficiency is largest when the phase between the body and the vortices ranges from 0° to 45°. Here 0° means that the body reaches its maximum transverse displacement when one of the point vortices is at the same streamwise location. In other words, the zero phase brings the body as close to the point vortices as possible. Based on simulations at eight phases and at eight points in the six-dimensional parameter space, they indicated that input power and thrust are also largest for phases between 0° and 45°. However, when the body is closest to the clusters of point vortices, the error in representing a real viscous vortex by such a cluster becomes significant. In the linearized model, they found that the optimal efficiency phase ranged from 0° down to about −90° as they varied the strength of the vortex street.

The same phenomenon was studied experimentally by Liao *et al.* (2003). They produced a von Kármán street using a steady flow past a D-shaped cylinder, and placed a rainbow trout in the wake of the flow. They found that the trout maintained its streamwise position relative to the cylinder while 'slaloming' in between the vortices. When a given vortex approached, the trout swam around it, moving transversely away from the vortex. This motion, which was presented as the characteristic swimming motion for the trout in the vortex street, corresponded to a range of phase differences between different points on the fish body and the vortex street. The phases ranged from $\pi/2$ at the head to near $3\pi/2$ at the tail. They also found a decrease in muscle activity during the motion, supporting the notion of an increased efficiency. This experiment indicates that an actual fish may swim with a phase relative to the vortex street which is very different from the optimal phases of Streitlien *et al.* (1996). In general, the trout moves transversely away from the vortices while the simulations show that a motion towards the vortices is better. A more extensive study appeared in Beal *et al.* (2006), which interpreted the thrust gain in terms of body-vortex interactions. Also relevant are two studies of passive body motions near vorticity: Eldredge & Pisani (2008) studied computationally the passive motion of a linked rigid body in the viscous wake of a cylinder, and Kanso & Oskouei (2008) studied the passive motion of a rigid ellipse near two oppositely signed point vortices.

Here we propose a new theoretical model of a body swimming in a vortex street, different from the model studied by Streitlien *et al.* (1996) and amenable to analytical calculation. Analytical methods are made possible by restricting to the limit where the amplitude of body motion is small relative to the streamwise and transverse spacing of the vortex street. By considering a periodic body, we avoid free distributions of vorticity shed from the body and the complications inherent in their simulation using the Kutta condition (Shukla & Eldredge 2007; Alben & Shelley 2008). We use the Hilbert transform to obtain the power output and efficiency as approximate or exact functions of the dimensionless parameters. Like previous models of this problem, ours assumes a two-dimensional inviscid flow.
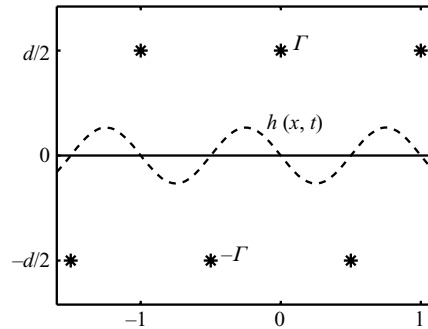
FIGURE 1. The parameters for a body swimming with amplitude $h(x, t)$ in a vortex street with width d, horizontal spacing between vortices l. A background flow velocity $U e_x$ is assumed.

An outline of subsequent sections of the paper is as follows. In §2, we derive the leading-order modification to the flow due to the swimming body, which is the same as that due to a horizontal sheet. The effect is to uniformly speed up the reverse von Kármán vortex street and to slow down the regular von Kármán street. In §3 we derive analytical formulas for the leading-order vorticity distribution and pressure jump along the body, and the resulting input and output power needed to maintain a given swimming motion. We use these formulas to find optimal swimming motions for two simple problems in §4. In the first problem, we find the travelling-wave motion which maximizes output power among motions with a fixed amplitude. This identifies a particular shape of the body which produces large thrust. The optimal shape is simply proportional to the first derivative of the pressure distribution. The output power can be found exactly, and shows a transition from a power law behaviour for narrow vortex streets to an exponential behaviour for wide vortex streets. The phase difference between the optimal shape and the vortex street varies smoothly from $0°$ in the limit of zero vortex street width to $90°$ (saturation) at an intermediate vortex street width. The Froude efficiency is found to be the same for all travelling-wave shapes with the same spatial and temporal frequency as the vortex street. For a reverse von Kármán street, weaker and wider vortex streets allow for higher efficiencies. Stronger and narrower streets yield higher efficiencies for the regular von Kármán street, up to a limiting vortex strength. We also consider another measure of efficiency, which is the amount of vortex street energy recovered by a foil per unit time. This efficiency turns out to be proportional to output power for travelling-wave shapes. In the second problem, we include internal damping due to Kelvin–Voigt viscoelastic behaviour. Optimal efficiency shapes are smoothed versions of the pressure profile, and efficiency shows an algebraic dependence on the damping parameter, and an exponential decay for wider vortex streets relative to the undamped efficiency. In §5 we make some comments on the body's effect on stability of vortex streets. Finally, §6 compares our main results with those of previous experiments and simulations.

2. Periodic flexible body in a vortex street

We consider a periodic flexible body in a periodic von Kármán vortex street. The street consists of two alternating rows of vortices (see figure 1). The top row has identical point vortices, each with circulation Γ, at the points $\{ml + \mathrm{i}d/2, m \in \mathbb{Z}\}$. The bottom row has vortices with circulation $-\Gamma$ located at the points $\{(m + 1/2)l - \mathrm{i}d/2, m \in \mathbb{Z}\}$. The spacing between neighbouring vortices in a row is then l, and the

width of the vortex street is d. For the regular von Kármán street, $\Gamma < 0$, while for the reverse von Kármán street, $\Gamma > 0$ (positive Γ corresponds to counterclockwise rotation). We assume that the point vortices are superposed on a background flow with uniform speed U. Such is the case when vortices are shed from a stationary body in a uniform stream, or from a body swimming at constant speed through quiescent fluid. In the latter case the background flow velocity is the negative of the body velocity, when we view the vortex street in a reference frame translating with the swimming body. In the unbounded plane, the vortex street translates with uniform velocity $U_c e_x$ given by Saffman (1992):

$$U_c = U + (\Gamma/2l)\tanh(\pi d/l). \tag{2.1}$$

We now introduce a flexible body in the form of an infinite sheet along the midline between the two alternating rows of vortices. The sheet executes small-amplitude displacements $h(x, t)$ transverse to the mid-line, and thus has complex position $x + ih(x, t)$, $|h/l| \ll 1$.

We consider first the undeflected 'base state' in which the infinite flexible solid sheet lies exactly along the x-axis. The condition that fluid does not penetrate the body can be satisfied by posing a vortex sheet, or equivalently a jump in tangential velocity, across the body. The strength distribution of the vortex sheet is set to cancel the vertical velocity along the body induced by the translating vortex street. We shall determine the strength of the vortex sheet in the base case, which is accurate up to $O(|h/l|, |\partial_x h|)$ in an expansion in powers of $|h/l|$ and $|\partial_x h|$. We shall also show that it modifies the velocity of the vortex street uniformly to a new constant velocity $U_s e_x$.

Let us first consider the flow induced by the von Kármán street alone. At the instant when one of the vortices in the top row lies on the y-axis, the flow has the following complex velocity potential (Saffman 1992):

$$w = Uz + \frac{-i\Gamma}{2\pi}\log\left(\sin\left(\frac{\pi}{l}\left(z - \frac{id}{2}\right)\right)\right) + \frac{i\Gamma}{2\pi}\log\left(\sin\left(\frac{\pi}{l}\left(z + \frac{l}{2} + \frac{id}{2}\right)\right)\right). \tag{2.2}$$

The complex–conjugate velocity is

$$u - iv = \frac{dw}{dz} = U - \frac{i\Gamma}{2l}\cot\left(\frac{\pi}{l}\left(z - \frac{id}{2}\right)\right) + \frac{i\Gamma}{2l}\cot\left(\frac{\pi}{l}\left(z + \frac{l}{2} + \frac{id}{2}\right)\right). \tag{2.3}$$

Evaluating (2.3) at $z = x$ and simplifying, we find that the conjugate flow velocity on the x-axis is

$$u - iv|_{y=0} = U - i\frac{\Gamma}{l}\frac{\cosh(\pi d/l)}{\sin(2\pi x/l) - i\sinh(\pi d/l)}. \tag{2.4}$$

Separated into real and imaginary parts, (2.4) reads

$$u|_{y=0} = U + \frac{\Gamma}{l}\frac{\sinh(\pi d/l)\cosh(\pi d/l)}{\sin^2(2\pi x/l) + \sinh^2(\pi d/l)}, \tag{2.5}$$

$$v|_{y=0} = \frac{\Gamma}{l}\frac{\sin(2\pi x/l)\cosh(\pi d/l)}{\sin^2(2\pi x/l) + \sinh^2(\pi d/l)}. \tag{2.6}$$

In what follows it is convenient to write v in (2.6) as a sine series:

$$v|_{y=0} = \frac{\Gamma}{l}\sum_{k=1}^{\infty} v_k \sin(2\pi k x/l). \tag{2.7}$$

It turns out that only odd-k coefficients are non-zero in (2.7).

The vertical velocity induced by the vortices is cancelled by the vertical velocity $-v$ due to the vortex sheet along the horizontal body $\gamma(x)$, which satisfies (Batchelor 1967):

$$-v = \frac{1}{2\pi} \int_{-\infty}^{\infty} \frac{\gamma(x')\,\mathrm{d}x'}{x - x'} = \frac{1}{2} H(\gamma). \tag{2.8}$$

Here H denotes the Hilbert transform. Using the identity

$$H(\mathrm{e}^{\mathrm{i}kx}) = -\mathrm{i}\,\mathrm{sign}(k)\mathrm{e}^{\mathrm{i}kx}, \tag{2.9}$$

the γ in (2.8) corresponding to v in (2.7) is

$$\gamma = -\frac{2\Gamma}{l} \sum_{k=1}^{\infty} v_k \cos(2\pi kx/l) = -\frac{2\Gamma}{l} \frac{\cos(2\pi x/l)\,\sinh(\pi d/l)}{\sin^2(2\pi x/l) + \sinh^2(\pi d/l)}. \tag{2.10}$$

The last expression in (2.10) is obtained by explicitly evaluating the cosine series using the coefficients for v_k from (2.6) and (2.7) and trigonometric identities. This distribution of vorticity induces a velocity at the point vortices. This velocity is a contour integral:

$$u(x, y) - \mathrm{i}v(x, y) = \frac{1}{2\pi\mathrm{i}} \int_{-\infty}^{\infty} \frac{\gamma(x')\,\mathrm{d}x'}{x + \mathrm{i}y - x'} \tag{2.11}$$

$$= \frac{(-2\Gamma/l)}{2\pi\mathrm{i}} \sum_{k=1}^{\infty} v_k \int_{-\infty}^{\infty} \frac{(\cos(2\pi kx'/l))\,\mathrm{d}x'}{x + \mathrm{i}y - x'}. \tag{2.12}$$

Each integral in the sum (2.12) is a standard contour integral in the residue theory of complex integration (Ahlfors 1979). The integral is evaluated using separate contours when the target point is in the upper half-plane ($y > 0$) and when the target point is in the lower half-plane ($y < 0$). Each contour is closed, and consists of a long segment of the real axis ($-N < x < N$, $N \gg 1$) joined to a large semicircle in the upper half-plane (when $y > 0$ in (2.12)) or lower half-plane (when $y < 0$ in (2.12)). Taking the limit $N \to \infty$, the result is

$$u(x, y) - \mathrm{i}v(x, y) = \frac{\Gamma}{l} \sum_{k=1}^{\infty} v_k \mathrm{e}^{\mathrm{i}2\pi k(x + \mathrm{i}y)/l}, \qquad y > 0 \tag{2.13}$$

$$= -\frac{\Gamma}{l} \sum_{k=1}^{\infty} v_k \mathrm{e}^{-\mathrm{i}2\pi k(x + \mathrm{i}y)/l}, \qquad y < 0. \tag{2.14}$$

For the upper row of vortices $x + \mathrm{i}y = ml + \mathrm{i}d/2, m \in \mathbb{Z}$, while for the lower row of vortices $x + \mathrm{i}y = (m + 1/2)l - \mathrm{i}d/2, m \in \mathbb{Z}$. The velocity induced by the vortex sheet (defined in (2.14)) is the same at all point vortices, and is

$$U_{ind} = \frac{\Gamma}{l} \sum_{k=1}^{\infty} v_k \mathrm{e}^{-\pi kd/l}. \tag{2.15}$$

U_{ind} can be written as the value of an analytic function at $z = id/2$:

$$U_{ind} = f(z)|_{z=id/2}, \qquad (2.16)$$

$$f(z) = \frac{\Gamma}{l} \sum_{k=1}^{\infty} v_k e^{2\pi ikz/l}, \qquad (2.17)$$

$$= \frac{\Gamma}{l} \sum_{k=1}^{\infty} v_k (\cos(2\pi kz/l) + i\sin(2\pi kz/l)). \qquad (2.18)$$

We already have an expression for $f(z)$ restricted to the real line $z = x$. The imaginary part of $f(x)$ is given by (2.6) and (2.7), and the real part is given by (2.10). Then $f(z)$ is the unique analytic extension of $f(x)$ to its maximum domain of analyticity (Ahlfors 1979). Inserting z for x in $f(x)$, and evaluating the result at $z = id/2$, we obtain

$$U_{ind} = \frac{\Gamma}{l} \frac{1}{\sinh(2\pi d/l)}. \qquad (2.19)$$

Since U_{ind} is a constant, the infinite horizontal sheet simply adds a uniform horizontal velocity to the vortex street but does not alter its spatial structure. The sheet adds negative horizontal velocity to the regular von Kármán street and positive horizontal velocity to the reverse von Kármán street; the velocity increment has the same sign as that induced by the point vortices on each other. Thus with the speed of the vortex street given by

$$U_s = U_c + U_{ind} = U + \frac{\Gamma}{2l} \tanh(\pi d/l) + \frac{\Gamma}{l} \frac{1}{\sinh(2\pi d/l)}, \qquad (2.20)$$

$$= U + \frac{\Gamma}{2l} \coth(\pi d/l), \qquad (2.21)$$

we obtain a self-consistent base state for the vortex street motion about a body on the horizontal axis. The velocity of the vortex street diverges as $d/l \to 0$, because in this limit γ in (2.10) tends to a sequence of sharp peaks of vorticity, adjacent to and opposite in sign to the point vortices in the street. The speed of a pair of oppositely signed distributions of vorticity diverges as they approach one another. As $d/l \to \infty$, the vortex street speed converges to $U_s = U + \Gamma/2l$. This is the same as the speed of the vortex street in the absence of the horizontal sheet as $d/l \to \infty$.

We have so far given all flow variables as functions of x and z, which holds only at the instant when a vortex from the top row coincides with the y-axis. Because the point vortices translate horizontally with speed U_s, the flow variables u, v and γ are travelling waves with x changed to $x - U_s t$ in the expressions given so far (setting the temporal phase so that a vortex from the upper street crosses the y-axis at time $t = 0$). The unsteadiness of the flow affects the pressure, as we show in the next section.

3. Pressure force, input power and output power

Given the base state in which the body lies on the horizontal axis and the vortex street translates with velocity U_s given by (2.21), we now consider prescribed motions of the body and calculate the resulting thrust force per unit length on it.

First, because we are interested in body motions with the same length scale as the spacing between neighbouring vortices, we assume that the motion has the same spatial period as the vortex street (l). We make the further simplifying assumption – in agreement with Streitlien *et al.* (1996) and Liao *et al.* (2003) – that the body motion

is a travelling wave moving with the speed of the vortex street U_s. When viewed in the rest frame of the vortex street, the body thus takes a constant shape.

We now make the assumption that the body executes small-amplitude motions $h(x, t)$, so that $|h| \ll l$, $|\partial_x h| \ll 1$. Then we can proceed to compute the pressure jump $[p]$ across the body, accurate to $O(|h|/l, |\partial_x h|)$, as simply that across the undeflected sheet. This provides the leading-order term in expansions of the power output P_{out} due to thrust forces on the body, and the power input P_{in} due to the work done by the body against fluid pressure forces. We now compute the leading-order terms in $[p]$, P_{out} and P_{in}.

3.1. *Pressure jump*

We begin by noting that for transverse body motions $h(x, t)$, the velocity induced by the point vortices at the body is given by the complex conjugate of (2.3) with $z = x + ih(x, t)$. The component of this velocity normal to the body is given by the real part of its product with the quantity $(-\partial_x h - i)/\sqrt{1 + \partial_x h^2}$. Up to $O(|h|/l, |\partial_x h|)$, the normal component is the same as v in (2.6). The vortex sheet strength γ is then computed from the first (2.8) with x' changed to $x' + ih(x', t)$. The result is again (2.10) up to $O(|h/l|)$. This γ is then used in (2.12) to compute the velocity induced by the vortex sheet at the point vortices, with x' changed to $x' + ih(x', t)$. The result is again an $O(|h/l|)$ correction, so body movements do not alter the motion of the vortex street at $O(1)$.

Thus the leading-order contribution to the vortex sheet strength on the body is γ from (2.10). We can calculate the pressure jump across a body supporting a vortex sheet in terms of the vortex sheet strength γ. One writes the Euler equation on both sides of the sheet, and takes the difference of the tangential components of the fluid acceleration terms on the either side of the body. This is done as in Saffman (1992, p. 31). The result is

$$\gamma_t + \partial_s((\mu - \tau)\gamma) = \frac{1}{\rho_f} \partial_s [p], \tag{3.1}$$

where s is arclength along the body, ρ_f is the fluid density, $\tau(s, t)$ is the tangential component of the body velocity and $\mu(s, t)$ is the tangential component of the average $w(s, t)$ of the fluid velocities on the two sides of the body at s:

$$\tau(s, t) = \text{Re} (\partial_t \zeta(s, t) \bar{s}); \quad \mu(s, t) = \text{Re} (w(s, t) \bar{s}). \tag{3.2}$$

Here the body position is the complex-valued function $\zeta(s, t)$. The tangent vector is

$$s = (1 + i\partial_x h)/\sqrt{1 + \partial_x h^2}. \tag{3.3}$$

Thus the tangential velocity due to the vertical motion $h(x, t)$ is $\tau = \partial_t h \partial_x h / \sqrt{1 + \partial_x h^2} = O(|\partial_x h|^2)$. The average fluid velocity at the body is horizontal in the base state (where the body is horizontal), and is the expression given in (2.5), a superposition of the background flow speed U plus the contribution from the point vortices:

$$\mu = U + \frac{\Gamma}{l} \frac{\sinh(\pi d/l) \cosh(\pi d/l)}{\sin^2(2\pi(x - U_s t)/l) + \sinh^2(\pi d/l)}. \tag{3.4}$$

To order $|\partial_x h|^2$ the s derivatives in (3.1) are x derivatives, and the equation becomes

$$\partial_t \gamma + \partial_x(\mu \gamma) = \frac{1}{\rho_f} \partial_x [p]. \tag{3.5}$$
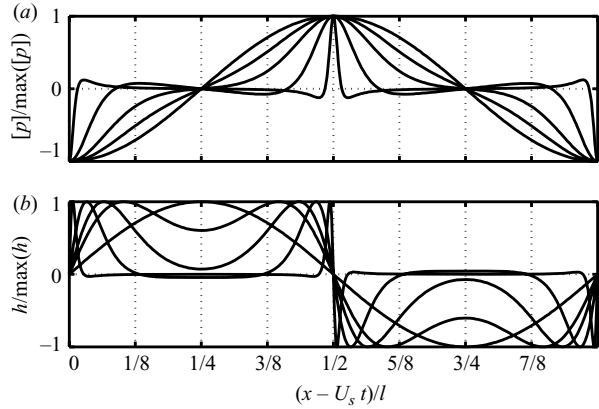
FIGURE 2. (*a*) The pressure jump profile for five values of $\pi d/l = 0.1, 0.5, 1, 1.5, 5$. The *x*-axis tick labels are the same as in (*b*). (*b*) The optimal swimming shapes *h* for the same values of $\pi d/l$, given by (4.3).

The instant $t = 0$ is assumed for γ in (2.10). The time-dependent γ is the same but with *x* replaced by $x - U_s t$. Because γ is a travelling wave,

$$\partial_t \gamma = -U_s \partial_x \gamma. \tag{3.6}$$

and thus the solution to $[p]$ in (3.5) is

$$[p] = \rho_f(\mu - U_s)\gamma. \tag{3.7}$$

$$= -\rho_f \frac{\Gamma^2}{l^2} \left[\frac{\sinh(\pi d/l)\cosh(\pi d/l) - \coth(\pi d/l)\sin^2(2\pi(x - U_s t)/l)}{(\sin^2(2\pi(x - U_s t)/l) + \sinh^2(\pi d/l))^2} \right]$$
$$\times (\cos(2\pi(x - U_s t)/l)\sinh(\pi d/l)). \tag{3.8}$$

We note that the pressure jump is independent of the background flow speed *U* at leading order, unlike in previous studies of slender bodies nearly aligned with flows such as a flapping flag (Shelley, Vandenberghe & Zhang 2005; Alben & Shelley 2008). The reason is that the body is undeflected in the base state, so superposing a horizontal background flow changes the flow velocity and also the fluid pressure equally above and below the body. Hence the difference in pressures is not affected by *U* at leading order in body deflection.

In figure 2(*a*) we plot $[p]$ for five different values of d/l. When the vortices are far from the swimming sheet (d/l is large), the pressure jump profile tends to a cosine function. As d/l decreases, the pressure jump becomes localized as sharp peaks at the horizontal location of the point vortices, and is relatively flat between the peaks.

3.2. *Input power*

Motion of the body normal to itself requires an input power per unit area p_{in} equal to the product of velocity in the normal direction with $[p]$, the force per unit area in the normal direction against which the body works. At a fixed point on the body this is

$$p_{in} = [p]\text{Im}\left(\partial_t \zeta(s, t)\,\bar{s}\right), \tag{3.9}$$
$$= [p]\partial_t h(x, t)(1 + O(|\partial_x h|^2)), \tag{3.10}$$

using (3.3). We integrate over the period length $0 \leqslant x < l$ to obtain the input power per period length, and per unit width in the third dimension:

$$P_{in} = \int_0^l [p] \partial_t h(x, t) \, \mathrm{d}x. \tag{3.11}$$

3.3. *Output power*

The thrust force per unit area f_{out} is given by the negative of the horizontal component of the body normal times the negative of the pressure jump:

$$f_{out} = -[p] \mathrm{Re}(\hat{n} \cdot -\hat{e}_x), \tag{3.12}$$
$$= -[p] \partial_x h / \sqrt{1 + \partial_x h^2}, \tag{3.13}$$
$$= -[p] \partial_x h + O(|\partial_x h|^3). \tag{3.14}$$

If we consider the problem in the frame in which the background flow is at rest, the body moves upstream at a prescribed velocity $-U e_x$. The work done on the body per unit time (power) per unit area in this frame by the thrust force per unit area (3.14) is p_{out}, at leading order:

$$p_{out} = -U[p] \partial_x h(x, t), \tag{3.15}$$

$$P_{out} = -U \int_0^l [p] \partial_x h(x, t) \, \mathrm{d}x. \tag{3.16}$$

P_{out} is the output power per unit period length, per unit width in the third dimension. Similar expressions for P_{in} and P_{out} were used in theoretical studies of fish swimming by Lighthill (1960) and Wu (1961). Because $[p]$ and h are both travelling waves with the same spatial and temporal period, so are the products in the integrands of P_{in} and P_{out}. As time evolves, the periodic integrands simply shift within the interval $[0, l]$, so P_{in} and P_{out} are constant in time, and thus their time averages are the quantities themselves.

We now consider constrained optimization problems which identify optimal swimming motions $h(x, t)$.

4. Optimal motions

4.1. *Fixed mean square amplitude*

We first compute the shapes which maximize power output for a given mean square amplitude. This identifies a particular body shape, independent of amplitude, for delivering large thrust. We thus maximize the functional

$$L_1 = P_{out} + \lambda \left(A^2 - \frac{1}{l} \int_0^l h(x', t)^2 \, \mathrm{d}x' \right), \tag{4.1}$$

where P_{out} is given by (3.16) and A is the mean square amplitude. Inserting $h \sim A$ into (3.16), and examining the form of $[p]$ (defined in (3.8)), we see that $P_{out}/\rho_f A$ is a function of four parameters: Γ, l, U, d. From these we form two dimensionless parameters for this problem: $\Gamma/lU, d/l$. In the following we shall see that only the dependence on d/l is non-trivial.

Taking the variation of (4.1) with respect to h and integrating by parts,

$$\delta L_1 = \int_0^l U \partial_x [p] \delta h(x', t) \, \mathrm{d}x' - \lambda \left(\frac{1}{l} \int_0^l 2h(x', t) \delta h(x', t) \, \mathrm{d}x' \right). \tag{4.2}$$
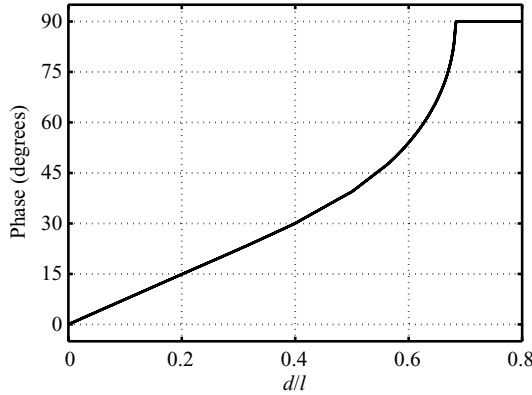
FIGURE 3. The phase between the vortex street and the maximum transverse displacement of the optimal-power-output shape $h(x, t)$, versus the vortex street width parameter d/l.

The maximizing h is given by

$$h(x, t) = A\partial_x[p] \left/ \sqrt{\frac{1}{l} \int_0^l (\partial_x[p])^2 \, \mathrm{d}x'}\right. . \tag{4.3}$$

In figure 2 we plot h and $[p]$ for different values of d/l. We see that as the point vortices approach the body, h becomes an increasingly concentrated bump near the point vortices, where the pressure jump is largest. Streitlien *et al.* (1996) found in some cases that power output is maximum when the phase difference between the foil (at its maximum transverse displacement) and the vortex street is near zero. Here the phase difference is the horizontal distance between a point vortex in the upper row of vortices and the nearest peak in $h(x, t)$ downstream (see figure 2*b*).

In figure 3 we plot the phase difference between the peak of the optimal body shape and the vortex street. We plot the phase difference in degrees, where $360°$ equals one spatial period. The phase difference moves gradually from 0 when $d/l = 0$ to $90°$ when $d/l = 0.684$. Above this value of d/l, the two peaks of h which occur in the range $0 \leqslant (x - U_s t)/l \leqslant 1/2$ in figure 2(*b*) have merged into a single peak at $(x - U_s t)/l = 1/4$.

The value of P_{out} generated by the P_{out}-maximizing shape (4.3) is

$$P_{out} = U A l \sqrt{\frac{1}{l} \int_0^l (\partial_x[p])^2 \, \mathrm{d}x'}. \tag{4.4}$$

Because $[p]$ in (3.8) is a rational expression of trigonometric functions, so is h in (4.3) and so is the integrand of the maximum output power (4.4). It is possible to compute the maximum output power in closed form using a symbolic integration package. Here we use Mathematica 6. The result is

$$P_{out} = \rho_f U A \frac{\Gamma^2}{l^2} \sqrt{\frac{\pi(115 + 76\cosh(4d\pi/l) + \cosh(8d\pi/l))}{\sinh(2d\pi/l)^5}}. \tag{4.5}$$

In figure 4 we plot P_{out} versus d/l. For large d/l, the power output decays exponentially:

$$P_{out} = \rho_f U A \frac{\Gamma^2}{l^2} 2\sqrt{\pi} \mathrm{e}^{-d\pi/l} + O(\mathrm{e}^{-2d\pi/l}), \qquad \frac{d}{l} \to \infty, \tag{4.6}$$
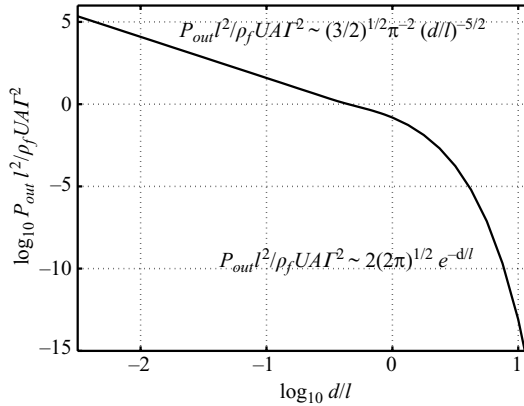
FIGURE 4. The dimensionless output power delivered by the optimal swimming shape, versus the vortex street width parameter d/l.
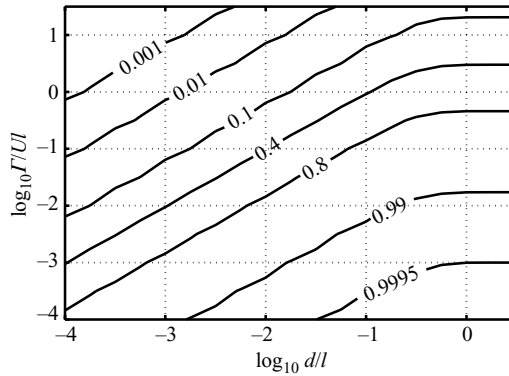

FIGURE 5. A contour plot of optimal Froude efficiency η relative to the dimensionless circulation Γ/lU and vortex street width d/l, for the reverse von Kármán street ($\Gamma > 0$).

while for small d/l the power out diverges like a power law, as the sheet deformation becomes localized near the point vortices:

$$P_{out} = \rho_f U A \frac{\Gamma^2}{\pi^2 l^2} \sqrt{\frac{3}{2}} \left(\frac{d}{l}\right)^{-5/2} + O\left(\left(\frac{d}{l}\right)^{-1/2}\right), \qquad \frac{d}{l} \to 0. \tag{4.7}$$

There is a smooth transition from one regime to the other near $d = l$.

We now consider the question of Froude efficiency. It turns out that all travelling-wave body shapes $h(x - U_s t)$ have the same Froude efficiency, or else P_{in} and P_{out} are zero. This follows from the fact that $\partial_t h = -U_s \partial_x h$. By the definitions of P_{out} and P_{in},

$$\eta = P_{out}/P_{in} = U/U_s = \left(1 + \frac{\Gamma}{2lU} \coth(\pi d/l)\right)^{-1}. \tag{4.8}$$

Because of the travelling-wave form of h and $[p]$, both P_{out} and P_{in} are proportional to the correlation between the slope of the body shape wave and the pressure wave. All travelling waves have the same such correlation.

In figure 5 we plot contours of constant η in the two-parameter space of reduced vortex circulation and reduced vortex street width, for the case $\Gamma > 0$. High efficiency

occurs with very weak vortices (small Γ/lU). Weaker vortices also result in a slower-moving vortex street. Thus the velocity of the body wave is smaller, leading to a smaller P_{in}. Conversely, stronger vortices require the body wave to move more quickly, which increases P_{in} (by increasing $\partial_t h$) and decreases the efficiency. Efficiency increases as the vortex street becomes wider, up to a critical value of d/l near 1, where the efficiency approaches a constant limiting value.

Our expressions for $[p]$ and P_{out} involve Γ only as Γ^2, and thus are the same for regular and reverse von Kármán streets. Our expression for Froude efficiency (4.8) involves the first power of Γ, however, and can be greater than 1 for a regular von Kármán street ($\Gamma < 0$), while it is always less than 1 for a reverse von Kármán street ($\Gamma > 0$). When $\Gamma < 0$ Froude efficiencies greater than 1 are common (Streitlien *et al.* 1996), and the term 'efficiency' is perhaps misleading because the body does no work in setting up the vortex street, but gains output power from it. It is then useful to consider an alternative definition of efficiency, which is the amount of kinetic energy in the vortex street recovered by the body per period length, per unit time (Streitlien *et al.* 1996):

$$\eta_1 = \frac{P_{out} - P_{in}}{U\langle D\rangle}, \tag{4.9}$$

where $\langle D\rangle$ is the time-averaged drag force on the object which sheds the vortex street. The outward momentum flux due to the point vortices leaving a control volume around the object is used to calculate $\langle D\rangle$ (Saffman 1992):

$$\langle D\rangle = \frac{\Gamma^2}{2\pi l} + \frac{\Gamma d}{l}(U - 2U_c). \tag{4.10}$$

Because the body is a travelling wave, $P_{in} = (U_s/U)P_{out}$ and

$$\eta_1 = \frac{(U - U_s)P_{out}}{U^2\langle D\rangle}. \tag{4.11}$$

Maximizing η_1 is thus equivalent to maximizing P_{out}, which we have already done under the constraint of fixed amplitude.

4.2. *Maximum efficiency with internal damping*

Thus far we have considered only the interaction of a flexible surface with an external flow due to a vortex street. We have neglected the internal work required for the body to perform a given motion. The muscles, tissues and organs of the fish body provide considerable resistance to bending (Videler 1993; Long *et al.* 1996), and evidence exists that the elastic properties of the fish body are tuned to hydrodynamic forces (Long *et al.* 1996; Wainwright 2000; Beal *et al.* 2006). One of the most basic ways to consider the effect of the internal resistance to bending is to model the fish as a beam with bending rigidity (Cheng, Pedley & Altringham 1998). Here we incorporate a uniform bending rigidity into our model of the flexible body, and show how the required input power and achievable efficiency is altered.

For a periodic beam with uniform flexural rigidity B, the stored elastic energy per period length l is

$$E_b = \frac{B}{2}\int_0^l (\partial_{xx}h(x',t))^2\,\mathrm{d}x'. \tag{4.12}$$

Because the motion $h(x,t)$ is periodic in time, E_b does not change over one period. Hence bending rigidity alone does not affect the time-averaged input power. However, real elastic structures also have internal damping, which can be modelled as internal

viscoelastic behaviour. One of the simplest and most widely used models for this phenomenon is the Kelvin–Voigt model, in which the stress tensor is a linear combination of the strain tensor and the rate-of-strain tensor (Banks & Inman 1991; Cheng *et al.* 1998). The result is a term proportional to $\partial_{txxxx}h$ in the beam equation (assuming spatially uniform damping):

$$\rho\partial_{tt}h + B\partial_{xxxx}h + c\partial_{xxxxt}h = f(x,t). \tag{4.13}$$

Here ρ is beam mass per unit length, c is the non-negative damping coefficient, and f is an applied force per unit length:

$$f(x,t) = -[p](x,t) + \partial_{xx}M_{int}(x,t), \tag{4.14}$$

where $[p]$ is the pressure jump (3.8) and M_{int} is the internal moment which produces the prescribed motion $h(x,t)$. Specifically $M_{int}(x,t)$ is the moment that material in the interval $\{x' : x' > x\}$ applies to the material in the interval $\{x' : x' < x\}$, in the notation of standard beam theory (Segel 1977). The alternating contraction of muscle fibres on either side of the fish backbone is the source of M_{int}.

The sum of kinetic and elastic potential energy of the beam per unit periodic length is

$$W(t) = \int_0^l \left(\frac{\rho}{2}(\partial_t h(x',t))^2 + \frac{B}{2}(\partial_{xx}h(x',t))^2 \right) dx'. \tag{4.15}$$

The time derivative of W is

$$\frac{dW}{dt} = \int_0^l (\rho\partial_{tt}h(x',t)\partial_t h(x',t) + B\partial_{xxxx}h(x',t)\partial_t h(x',t)) \, dx', \tag{4.16}$$

$$= \int_0^l [-c(\partial_{xxt}h)^2 - [p]\partial_t h(x',t) \, dx' + \partial_{xx}M_{int}(x',t)\partial_t h(x',t))], \tag{4.17}$$

where we have used (4.13) and integration by parts (with periodic boundary conditions). Because the motion of the beam is periodic, the integral of dW/dt over one temporal period T is zero. Thus,

$$\int_0^T \int_0^l \partial_{xx}M_{int}(x',t')\partial_t h(x',t') \, dx' \, dt' = \int_0^T \int_0^l c(\partial_{xxt}h)^2 + [p]\partial_t h(x',t') \, dx' \, dt'. \tag{4.18}$$

The quantity on the left is the time-averaged internal power per spatial wavelength used to maintain the motion $h(x,t)$. We see that it is equal to the negative of the rate of energy dissipation in internal damping plus the time-averaged power applied against fluid pressure.

We thus modify the input power in (3.11) to take internal damping into account:

$$P'_{in} = \int_0^l (c(\partial_{xxt}h)^2 + [p]\partial_t h(x',t')) \, dx'. \tag{4.19}$$

Equation (4.19) is equal to its time-average, because again we assume $h(x,t)$ is a travelling wave with spatial period l. We now maximize the efficiency

$$\eta' = P_{out}/P'_{in}. \tag{4.20}$$

In the limit where the amplitude of the body wave $\max_x |h(x,t)|/l$ goes to zero, the damping term in (4.19) becomes negligible and we recover the case where all body waves with non-zero power have the same efficiency U/U_s.

When we constrain the body wave to have a fixed positive power output, a particular body wave maximizes the efficiency η'. Thus we optimize

$$L_2 = P_{out}/P'_{in} + \lambda \left(S - \int_0^l -U\partial_x h[p]\,dx' \right),$$
(4.21)

where S is the fixed power output. Taking the variation of L_2 with respect to h and integrating by parts yields the equation for h:

$$\partial_x[p]\left(U P'_{in} - U_s P_{out} - \lambda U P'^2_{in}\right) = -2P_{out}cU_s^2\partial_x^6 h.$$
(4.22)

We find that h is proportional to the fifth antiderivative of $[p]$:

$$h = c_0 D^{-5}[p],$$
(4.23)

where negative powers of D denote antiderivatives, and c_0 is a constant to be determined. D^{-5} is a smoothing operator which damps the amplitudes of the cosine components of $[p]$ by wavenumber to the fifth power. Because $[p]$ contains only odd-wavenumber cosines, h is very well approximated by just the first cosine, $\cos(2\pi(x - U_s t)/l)$, scaled by a constant c_0 (the amplitude of the next cosine in $[p]$, $k=3$, is damped by a relative factor of 3^5). The constant c_0 is determined by inserting h into (3.16) and setting the power output equal to S:

$$c_0 = -S\left(U \int_0^l (D^{-2}[p])^2\,dx' \right)^{-1}.$$
(4.24)

The power input for the optimum efficiency solution is found by (4.19):

$$P'_{in} = \frac{SU_s}{U} + c\left(\frac{SU_s}{U}\right)^2 \left(\int_0^l (D^{-2}[p])^2\,dx'\right)^{-1}.$$
(4.25)

The corresponding efficiency is

$$\eta' = \frac{U}{U_s}\left(1 + cSU_s\left(U\int_0^l (D^{-2}[p])^2\,dx'\right)^{-1}\right)^{-1}.$$
(4.26)

By explicitly separating out the prefactor $\rho_f\Gamma^2/l^2$ from $[p]$ in (3.8), we can express the efficiency as a function of just two dimensionless parameters: d/l and a dimensionless damping constant $\bar{c}$:

$$\frac{U_s}{U}\eta' = (1 + \bar{c}f(d/l))^{-1},$$
(4.27)

$$\bar{c} = cSU_s l^4/(U\rho_f^2\Gamma^4),$$
(4.28)

$$f(d/l) = \frac{\rho_f^2\Gamma^4}{l^4}\left(\int_0^l (D^{-2}[p])^2\,dx'\right)^{-1}.$$
(4.29)

In the first optimization problem (§4.1) we found that only the dependence on a single parameter d/l was non-trivial. Considering the Froude efficiency (defined in (4.8)) then introduced a non-trivial dependence on a second parameter Γ/lU. By adding the damping constant c, we have obtained a third parameter $\bar{c}$ on which solutions depend non-trivially. Because Γ/lU appears only in U_s/U, we have absorbed it into η' (4.27) and $\bar{c}$. This allows us to plot solutions in terms of the two remaining parameters d/l and $\bar{c}$.
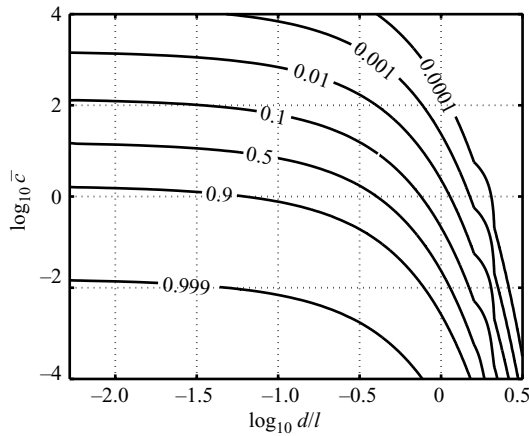
FIGURE 6. A contour plot of modified optimal efficiency $U_s\eta'/U$ (including internal damping, and for fixed power output S) relative to the dimensionless damping parameter $cSU_sl^4/(\rho_f^2\bar{U}\Gamma^4)$ and vortex street width d/l. Here η' is given as a fraction of the undamped efficiency U/U_s (defined in (4.8)).

The rescaling of efficiency in (4.27) is convenient because the scaling factor is the undamped efficiency U/U_s (defined in (4.8)). Thus we are naturally able to compare the two. In figure 6 we plot contours of constant $\eta'U_s/U$ given by (4.27) versus d/l and $\bar{c}$. The parameter $\bar{c}$ can be interpreted as a ratio of the characteristic input power required to balance internal damping to that required to work against the external fluid, for a body motion which produces output power S. First, we find unsurprisingly that $\eta'U_s/U \leqslant 1$; i.e. damped efficiency is always less than undamped efficiency. We find also that the efficiency decreases with increasing damping, as expected. As d/l exceeds 1, the efficiency decreases exponentially. The reason is that the amplitude of the pressure jump decreases exponentially as d/l exceeds 1. To obtain a fixed output power S, the amplitude of the body wave must then increase exponentially with d/l. This increases the damping term in P_{in} ((4.19) and (4.20)) at a higher exponential rate in d/l than it increases P_{out}. The result is an exponentially decreasing efficiency. Above $\log_{10} d/l = 0.5$, the amplitude $\max|h/l|$ approaches one, so the small-amplitude approximation is no longer valid for the optimal body waves.

We can understand the behaviour of optimal efficiency more quantitatively by an approximate analytical solution. We note that the operator D^{-2} also smoothes $[p]$ in η', though not nearly as much as for h. A good approximation to η' is obtained when we approximate $[p]$ in (3.8) by its first cosine component. Using Mathematica 6, this component is

$$[p] = \sum_{k=1}^{\infty} p_k \cos(2\pi k(x - U_s t)/l) \approx p_1 \cos(2\pi(x - U_s t)/l), \qquad (4.30)$$

$$p_1 = -2\frac{\rho_f\Gamma^2}{l^2}e^{-\pi d/l}. \qquad (4.31)$$

Using this approximation for $[p]$ in c_0 and h, h is approximately given by

$$\tilde{h} = \frac{Sl^2}{2\pi U\rho_f\Gamma^2}e^{\pi d/l}\sin(2\pi(x - U_s t)/l). \qquad (4.32)$$
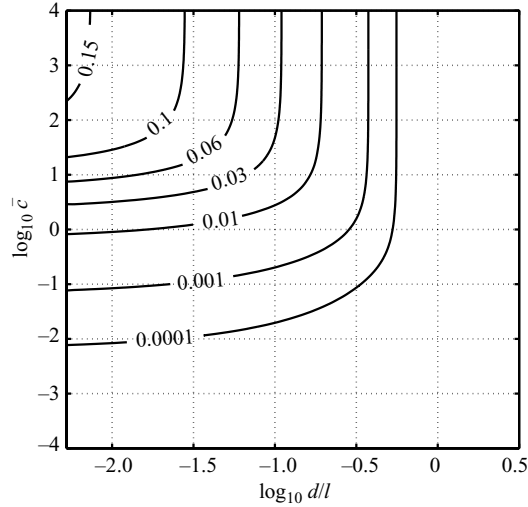
FIGURE 7. A contour plot of $|\tilde{\eta}' - \eta'|/|\eta'|$, the relative error in approximation (4.33) for η' (which includes just the first cosine mode of $[p]$). The contours are plotted in the space of the dimensionless damping parameter $\bar{c} = cSU_s l^4/(\rho_f^2 U \Gamma^4)$ and vortex street width d/l.

Here the phase difference between the vortex street and the approximate body shape is $\pi/2$, which is the same phase as for the maximum P_{out} body shape when d/l exceeds 0.684.

For the approximate $[p]$, η' becomes

$$\tilde{\eta}' = \frac{U}{U_s} \frac{1}{1 + (\bar{c}/4\pi)e^{4\pi d/l}}. \tag{4.33}$$

In figure 7 we plot the relative error in $\tilde{\eta}'$. We see that it is very small except for larger damping and smaller d/l. At smaller d/l the pressure peak becomes sharper (see figure 2), and higher frequencies become important. Thus retaining only the first cosine term can incur a significant error in this region. Because the damping constant multiplies the term which is approximated, there can only be a significant error when the damping constant is sufficiently large.

For the approximation $\tilde{\eta}'$, we can easily write down the asymptotic behaviour. For small vortex street width, the efficiency approaches a constant:

$$\tilde{\eta}' \sim \frac{U}{U_s} \frac{1}{1 + (\bar{c}/4\pi)}. \tag{4.34}$$

For large vortex street width, the efficiency decays exponentially with d/l:

$$\tilde{\eta}' \sim \frac{U}{U_s} \frac{4\pi}{\bar{c}} e^{-4d\pi/l}, \quad d/l \gg 1. \tag{4.35}$$

This gives a quantitative form for the exponential decay described qualitatively below (4.27).

5. Stability

In this work we have assumed that the body is periodic on the length of streamwise separation between vortices. Our intent is to model a body with length on the scale

of the streamwise spacing of vortices. It is also possible to apply our model to the case of a body which extends over a scale of many streamwise vortex spacings, and then it is interesting to consider whether or not such a body can stabilize the von Kármán vortex street through time-periodic motions. We note that in the literature there are relatively few experimental studies or natural observations of bodies of many vortex-spacings in length placed in a vortex street. Some studies have considered the behaviour of a vortex street in proximity to a solid wall (Bearman & Zdravkovich 1978; Zdravkovich 1983).

It is known that the von Kármán street is unstable to infinitesimal disturbances at all values of d/l but one, and unstable to finite disturbances at all values of d/l. These facts were reviewed by Saffman (1992), who also described models which try to understand why stable von Kármán streets are common at large but finite Reynolds number. It is an interesting topic for future work to determine the effect of an oscillating body on the stability of the von Kármán street. When the vortices are shed from a stationary body, a sufficiently large background flow, relative to the induced flow of the vortex street, i.e. $lU/\Gamma \gg 1$, can make any such instability a convective rather than absolute one.

There is some evidence which suggests that certain motions of a body near the centreline of a point-vortex street may stabilize it. Acton & Dhanak (1993) considered a lattice of sources on the midline of the vortex street, with a periodic distribution of source strength which moves downstream together with the vortex street. They motivated this problem as a basic one in flow control by using flow injection along a solid boundary. They found equilibria in which each vortex in the street executes small periodic motions superposed on constant downstream advection. The distribution of point source strength on the midline is chosen to be locked in phase to the periodic streamwise velocity of the vortex street. The combined flow due to the sources, vortex street, and uniform advection leads to a wavy streamline near the midline. This streamline can be interpreted as a 'virtual body' because fluid does not penetrate it. Acton & Dhanak (1993) found that when the phase between the virtual body amplitude and the vortex street is $\pi/2$, the combined motion is stable for certain ranges of the other dimensionless parameters. This is the same phase between the body and vortex street that we have found for optimal power output and efficiency in the case of wider vortex streets ($d/l \geqslant 0.684$) in §4.

6. Comparisons

We briefly compare some of our results with those of earlier work. First, our model predicts that P_{out} is maximized when the phase difference ranges from $0°$ (for small d/l) to $90°$ (for large d/l). Streitlien *et al.* (1996) considered a foil performing a combination of heaving and pitching. The trajectory traced by the foil over a time period is very similar to the shape assumed by our flexible sheet.

They did not report the values of d/l they used in simulations, but it can be estimated as 0.2 in their figure 4. For this d/l our model predicts an optimal phase of $15°$, while theirs is $20°$–$45°$ (figure 2 of Streitlien *et al.* 1996) for simulations with $A/d \leqslant 0.2$, which approximates the small-amplitude limit.

The linearized theory of Streitlien *et al.* (1996) did consider the small amplitude limit of their airfoil model, and the wide vortex street limit $d/l \rightarrow \infty$. Theirs was a regular von Kármán street, in which case our model predicts a Froude efficiency given by (4.8) with $\Gamma < 0$. They see an increased efficiency for increasing Γ/lU in their figure 3, which is also shown by our model in this case.

For rainbow trout swimming in a flow tunnel, Liao *et al.* (2003) found that the phase differences between the vortex and different locations on the trout body ranged from 90° to 270º(tail). From their PIV in figure 2, d/l can be estimated as 2/3. In this case, our first optimization predicts maximum P_{out} with 90° phase (for both the regular and reverse von Kármán streets), and our second optimization predicts maximum efficiency with the same phase. Our first comment is that the amplitude in the experiment is perhaps outside the small-amplitude limit. However, because the trout body always remains some distance from the vortices, our model is still reasonable. By matching optimal phases of the fish body and our model, our model suggests that the power savings due to the vortex street is more concentrated on the forward half of the trout (where the phase is closer to that of our optimal body shape) than in the posterior region. An alternative interpretation considers the mean phase of the trout, which is 180º. For this phase, our model predicts zero P_{in} (or, with damping, minimum P_{in}) and zero P_{out}. However, the trout possesses an additional means of generating thrust which is not present in our model – by shedding free vorticity into the fluid at the tail. With this addition to P_{out}, we would expect high efficiency at 180° phase. Apart from the free trailing wake, our periodic model also neglects leading-edge suction, and the free-edge boundary conditions appropriate to the edges of a finite swimming body.

REFERENCES

ABRAHAMS, M. V. & COLGAN, P. W. 1987 Fish schools and their hydrodynamic function: a reanalysis. *Environ. Biol. Fishes* **20** (1), 79–80.

ACTON, E. & DHANAK, M. R. 1993 The motion and stability of a vortex array above a pulsed surface. *J. Fluid Mech.* **247**, 231–245.

AHLFORS, L. V. 1979 *Complex Analysis*. McGraw-Hill.

ALBEN, S. & SHELLEY, M. J. 2008 Flapping states of a flag in an inviscid fluid: bistability and the transition to chaos. *Phys. Rev. Lett.* **100**, 074301.

BANKS, H. T. & INMAN, D. J. 1991 On damping mechanisms in beams. *J. Appl. Mech.* **58**, 716.

BATCHELOR, G. K. 1967 *An Introduction to Fluid Dynamics*. Cambridge University Press.

BEAL, D. N., HOVER, F. S., TRIANTAFYLLOU, M. S., LIAO, J. C. & LAUDER, G. V. 2006 Passive propulsion in vortex wakes. *J. Fluid Mech.* **549**, 385–402.

BEARMAN, P. W. & ZDRAVKOVICH, M. M. 1978 Flow around a circular cylinder near a plane boundary. *J. Fluid Mech.* **89**, 33–47.

CHENG, J.-Y., PEDLEY, T. J. & ALTRINGHAM, J. D. 1998 A continuous dynamic beam model for swimming fish. *Phil. Trans. R. Soc. Lond* B**353**, 981–997.

DRUCKER, E. G. & LAUDER, G. V. 2001 Locomotor function of the dorsal fin in teleost fishes: experimental analysis of wake forces in sunfish. *J. Exp. Biol.* **204** (17), 2943–2958.

ELDREDGE, J. D. & PISANI, D. 2008 Passive propulsion of a simple articulated system in the wake of an obstacle. *J. Fluid Mech.* **607**, 279–288.

KANSO, E. & OSKOUEI, B. G. 2008 Stability of a coupled body-vortex system. *J. Fluid Mech.* **600**, 77–94.

LIAO, J. C., BEAL, D. N., LAUDER, G. V. & TRIANTAFYLLOU, M. S. 2003 Fish exploiting vortices decrease muscle activity. *Science* **302** (5650), 1566–1569.

LIGHTHILL, M. J. 1960 Note on the swimming of slender fish. *J. Fluid Mech.* **9** (02), 305–317.

LISSAMAN, P. B. S. & SHOLLENBERGER, C. A. 1970 Formation flight of birds. *Science* **168** (3934), 1003–1005.

LONG, J., HALE, M., MCHENRY, M. & WESTNEAT, M. 1996 Functions of fish skin: flexural stiffness and steady swimming of longnose gar, *Lepisosteus osseus*. *J. Exp. Biol.* **199** (10), 2139–2151.

SAFFMAN, P. 1992 *Vortex Dynamics*. Cambridge University Press.

SEGEL, L. 1977 *Mathematics Applied to Continuum Mechanics*. Macmillan.

SHELLEY, M., VANDENBERGHE, N. & ZHANG, J. 2005 Heavy flags undergo spontaneous oscillations in flowing water. *Phys. Rev. Lett* **94**, 094302.

SHUKLA, R. K. & ELDREDGE, J. D. 2007 An inviscid model for vortex shedding from a deforming body. *Theor. Comput. Fluid Dyn.* **21** (5), 343–368.

STREITLIEN, K., TRIANTAFYLLOU, G. S. & TRIANTAFYLLOU, M. S. 1996 Efficient foil propulsion through vortex control. *AIAA J.* **34** (11), 2315–2319.

VIDELER, J. J. 1993 *Fish Swimming*. Springer.

WAINWRIGHT, S. A. 2000 The animal axis. *Am. Zool.* **40** (1), 19–27.

WEIHS, D. 1973 Hydromechanics of fish schooling. *Nature* **241** (5387), 290–291.

WEIMERSKIRCH, H., MARTIN, J., CLERQUIN, Y., ALEXANDRE, P. & JIRASKOVA, S. 2001 Energy saving in flight formation. *Nature* **413** (6857), 697–698.

WU, T. Y. 1961 Swimming of a waving plate. *J. Fluid Mech.* **10** (3), 321–344.

WU, T. Y. & CHWANG, A. T. 1975 Extraction of flow energy by fish and birds in a wavy stream. In *Swimming and Flying in Nature* (ed. T. Y. T. Wu, C. J. Brokaw & C. Brennen), vol. 2, pp. 687–702. Plenum Press.

ZDRAVKOVICH, M. M. 1983 Observation of vortex shedding behind a towed circular cylinder near a wall. In *Flow Visualization III: Proceedings of the Third International Symposium*. Ann Arbor, MI.